Seismic Behaviour of Complex H-Shaped Buried Structures

B. Salehi[1], A. Bahmanpour[2], and M. Derakhshandi[3]
[1]*Department of Civil Engineering, Science and Research Branch, Islamic Azad University, Tehran, Iran*
E-mail: aminbahmanpour@srbiau.ac.ir

ABSTRACT: Seismic loading parameters are always characterized by high complexity and uncertainty. The uncertainty increases in complex structures, which makes the process more complicated, particularly for structures that are partly buried deep and partly at the surface. In this research, the seismic behavior and stress changes of complex H-shaped structures have been studied using 2D FE analysis. Five points in the geometry of the model were selected at which the normal and shear stresses were extracted. Granular soil with variable strength parameters was investigated in the sensitivity analysis. The structures had height-to-width ratios of 1, 1.5 and 2. The results show that the stress increased in structures under near-field earthquake records. A decrease in shear stress was observed for all structural ratios with an increase in the internal friction angle. A rise in the internal friction angle at the midpoint of the wall also increased the shear stress. This growth was observed for all far-field earthquake records up to an internal friction angle of 35° and then descend. At a constant friction angle, climbing structure ratio H/L from 1 to 1.5 improved the shear stress at least 20%. However, as H/L changed from 1.5 to 2, the minimum stress increase was 85%. For far-field earthquakes, the stress values depended on the horizontal acceleration and H/L because they are influenced by the frequency content and internal friction angle.

KEYWORDS: Time history, Finite element method, Complex structure, Shear stress.

1. INTRODUCTION

Precise determination of the effect of dynamic loads, especially earthquakes, on geotechnical structures is associated with uncertainty. Surface structures such as retaining walls and buried structures such as tunnels require special attention because of their use in urban areas. A retaining wall can move or rotate under the influence of an earthquake and the relative displacement or rotation depends on the design of the wall. These effects can occur for specific walls (Nadim and Whitman, 1985) and both can be predicted (Seed et al., 1992). The amount and distribution of dynamic stress depends on the type of motion of the wall (Sherif et al., 1984).

Maximum soil movement on the wall occurs when it is rotated or moved toward the soil; that is, when an inertial force enters the wall in the opposite direction. Minimal soil drift occurs on the wall when it is rotated or moved away from the soil behind it. Okabe (1926) and Mononobe (1929) laid the foundations for quasi-static analysis of the seismic drift of a retaining structure, which is known as the Mononobe-Okabe (M-O) method.

Cakir and Livaoglu (2012) described a simple, efficient and reasonably accurate analytical model for the analysis of backfill-rectangular tank-fluid interaction systems. The results of parametric seismic analysis indicated that backfill interaction, wall flexibility and fluid interaction strongly affected lateral displacement. The sloshing response, however, was not practically affected by the backfill interaction and wall flexibility.

The seismic behavior of a tunnel depends on the geometric characteristics and structure of the tunnel as well as its relative hardness against the surrounding soil. The design of underground spaces without considering the seismic loads will lead to the construction of unsafe structures (Wang, 1993). On the other hand, when the seismic design of such spaces is done using common methods for surface structures, it will lead to an overly conservative design. Thus, the seismic design of such spaces should be based on specific principles.

There are various methods for analyzing and designing underground structures. The American Society of Civil Engineers (1974) examined the damage caused by the San Fernando earthquake in Los Angeles to underground structures and determined that seismic loads had a great effect on shallow tunnels.

The Japanese Society of Civil Engineers examined the performance of several underground structures, including tunnels with precast ring segments that had been affected by seismic loads. After the Kanuto earthquake, 82 out of 116 railroad tunnels in the region exhibited damage in the form of fracture of the portals, longitudinal and transverse fractures of the lining, scaling and deformation (Okamoto, 1984). Okamoto (1984) concluded that tunnel safety was related to dynamic ground parameters, but that weak geotechnical conditions in the soil/rock surrounding the tunnel could not be compensated for solely by increasing the lining thickness.

Owen and Scholl (1981) examined 127 circular and rectangular tunnels built using the cut-and-cover method with an emphasis on rectangular tunnels in weak soil. The results showed that the effect of the earthquake was intermittent with severe shocks. Because the surface structures were only connected to the ground at the lower surface, they were less resistant to the earthquake, but tunnels, which were in full contact with the surrounding environment, were more resistant.

Sharma and Judd (1991) reported on the behavior of 192 underground structures in 85 earthquakes worldwide. They created a database to determine the effect of various factors on the sustainability of underground spaces. They presented a relationship between maximum ground acceleration and the depth of the overburden to the amount of damage that can be used to estimate the initial tunnel stability before dynamic analysis.

Wang (1993) and Penzien (2000) used mathematical methods to estimate the forces applied to a tunnel lining under simplified loading for circular and rectangular tunnels. Hashash et al. (2001) compared the analytical relationships of Wang (1993) and Penzin (2009) using numerical finite element (FE) analysis. Wang (1993) approximated the earthquake load in the form of a centralized knot load or an inverted triangle, ignoring the effects of nonlinearity of the lining and soil behavior under seismic loads.

Dobashi et al. (2011) investigated the Japanese metro time-history. This structure consists of underground sections with twin tunnels and semi-surface station structures. The researchers concluded that the greatest effect from an earthquake in the longitudinal direction of the tunnel occurred at the portals. For the surface section, the structural performance was strongly dependent on the earthquake frequency and acceleration.

The present study investigated the stress on rectangular, complex, H-shaped underground structures using time-history analysis. The granular soil selected had a variable friction angle. For dynamic analysis, four far-field and four near-field earthquakes were selected and applied to the model. The structural dimensions are determined at height-to-width (H/L) ratios of 1, 1.5, and 2 for each case.

2. RESEARCH METHODOLOGY

2.1 Complex Structure

The behavior of geotechnical structures against earthquake forces is influenced by the parameters of the bed medium and the stiffness ratio between the structural materials and soil is a determining factor. The soil parameters are generally unchangeable and a structure should be designed according to the specific conditions. The ability to modify the geometry of a structure and the materials used to control the forces created in the structure is not usually available to engineers and researchers.

The behavior of deeply buried structures (such as a tunnel) differs from that of surface structures (such as retaining walls). When two structures are close together, the actual behavior must be scrutinized and, if necessary, new engineering design approaches should be applied.

A complex structure is a building that is partially constructed and operated at the surface and is partly underground. Examples of this include subway stations or tunnels and multi-floor ramps. Considering the increase of such structures in construction projects, this study investigated stress changes in these underground structures as influenced by earthquake-induced dynamic forces.

The selected geometry was of the regular type with variable dimension ratios. The width was assumed to be constant and the length of the structure varied from 10 to 20 m. Figure 1 shows the cross-section of the geometry of the structure. The middle beam was assumed to be in the middle of the structure. One-meter thick structural concrete and a 2.4×107 kPa elastic modulus were used for stabilization. The medium was a granular soil with the specifications given in Table 1. The internal friction angle was tested for 25° to 40° in 5° increments as a research variable.

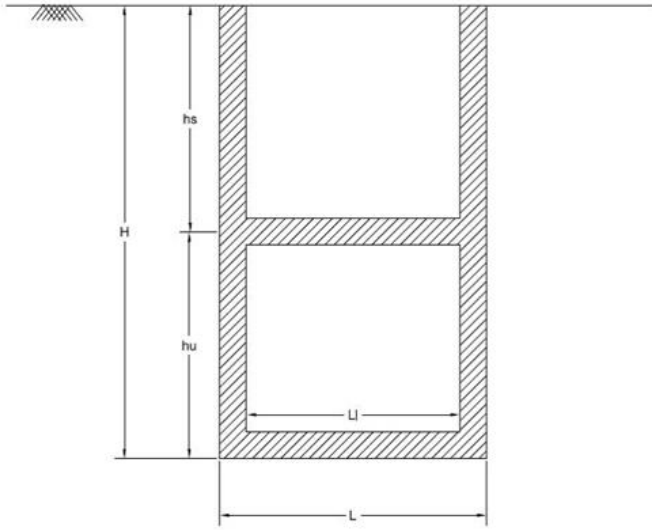

Figure 1 Cross-section of H-shaped complex structure

Table 1 Geotechnical characteristics of medium

Value	Parameter
hardening soil	behavioral model
25 to 40	friction
zero	cohesion
$1e_5$ kN/m^2	loading elastic modulus
$3e_5$ kN/m^2	unloading elastic modulus

The behavioral model selected was the hardening soil (HS) model. This nonlinear elasto-plastic model introduces the smallest changes in hardness depending on the range of strain changes and the results can be investigated by considering momentary changes. The HS model was designed by Schanz (1999) in order to reproduce the basic macroscopic phenomena exhibited by soil. It uses the same failure criteria as the Mohr-Coulomb model. Before reaching the failure surface, the HS model adopts a hyperbolic stress-strain relation between the normal strain and deviatory stress for primary loading as proposed by Duncan and Chang (1970). In the HS model, the soil stiffness can be calculated much more accurately using three types of stiffness: triaxial loading secant stiffness Eref50, triaxial unloading/reloading stiffness Erefur and oedometer loading tangent stiffness Eref oed.

Isotropic hardening of the HS model is connected to two plastic yield surfaces. The Mohr- Coulomb criterion (with mobilized friction) is represented as a “cone” which can expand gradually while loading towards failure. Unlike the Mohr-Coulomb model, the yield surface in the HS model is not fixed in a principle stress, but is able to expand because of plastic strain. The position of the pre-consolidation stress is a spherical surface or “cap”. The cap expands with an increase in pre-consolidation stress, which results in plastic volumetric strain (Nordal, 2016). Although this model provides greater accuracy than the Mohr-Coulomb model, it does not incorporate anisotropic strength-stiffness behavior, creep or time-dependent behavior of the soil and cyclic loading effect.

2.2 Design Earthquakes

FE analysis was performed in PLAXIS software. PLAXIS 2D is a two-dimensional finite element program developed for the analysis of deformation, stability and groundwater flow in geotechnical engineering (Brinkgreve et al., 2015). PLAXIS 2D models can be constructed as either in the plane-strain or axisymmetric conditions. It uses 6 or 15 nodal-point triangular elements to describe deformation. There are several material models that can be used to define the property of the soil. Structural elements such as plates, anchors, embedded beams and geogrids can be constructed.

Eight earthquake records, four near-field and four far-field, were used to investigate the performance of the H-shaped structure against dynamic loading (Figures 2 and 3). The seismic data was chosen from the PEER Ground Motion Database. The records were selected to have different maximum acceleration values. The distance from the epicenter of the earthquake was the mean criteria for the far- and near-field definitions used in this research. The RSN number represents the file number in the original data source.

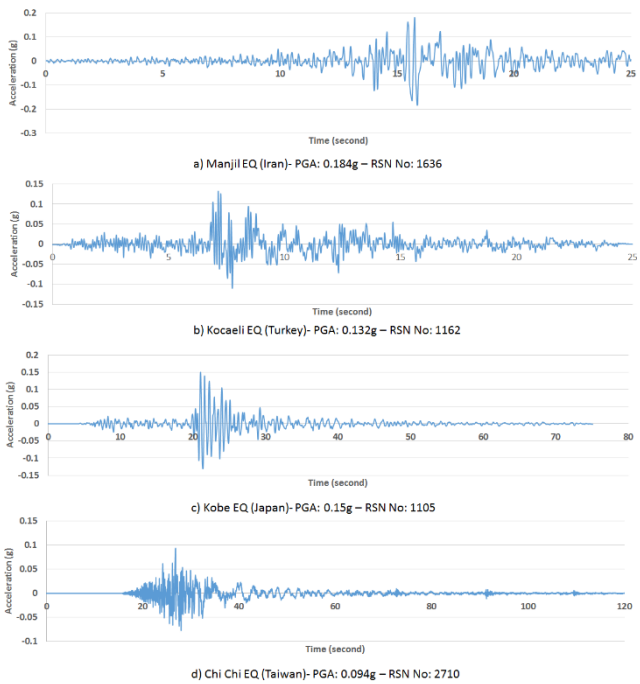

Figure 2 Far-field earthquake records used for FE analysis of models

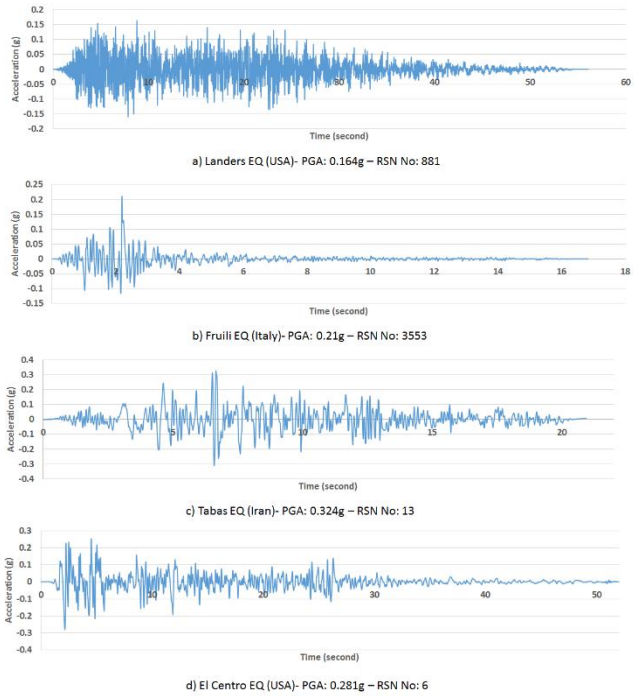

Figure 3 Near-field earthquake records used in FE analysis

2.3 Numerical Modelling

The tunnel structure and its surrounding soil were simultaneously simulated in PLAXIS The staged construction and continuous implementation of the lining of the H-shaped buried structure were in accordance with the actual construction stages and were taken into account in the model considering the initial stress conditions. In order to ensure the independence of the results from the model dimensions, two models were constructed, one of 30 × 60 m and 40 × 80 m. The models were solved using the Manjil earthquake record (horizontal seismic load) with an H/L = 1 aspect ratio and the output results were compared. The results of the shear stress variations at point M can be seen in Figure 4.

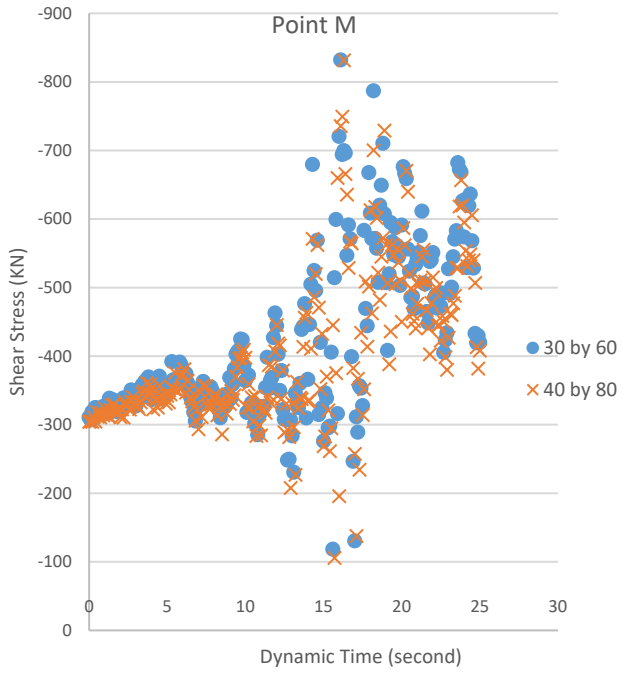

Figure 4 Effect of model dimensions on FE modeling results for Manjil earthquake

The difference in the root mean square deviation of the two geometries was approximately 4.2%. It is evident that the variation between the results was negligible. In order to avoid a direct effect from the model size and mesh number on the FE analysis time, the model with a width of 30 m and height of 60 m was constructed, as shown in Figure 5. When modeling the layers of soil, 15-node triangular elements and the HS model were used to examine the soil behavior.

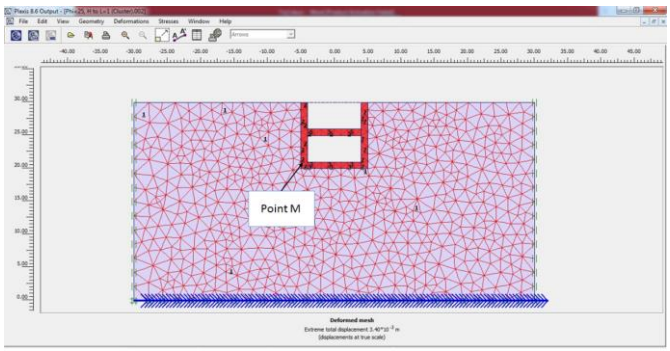

Figure 5 Geometry and meshing of FE model in PLAXIS

To investigate the accuracy of the modeling process, a physical model of the tunnel was simulated under dynamic loading. Lanazo et al. (2012) developed a physical model of a circular tunnel in granular soil and carried out a series of plane-strain centrifuge tests with dynamic loading on a model tunnel. Four samples of dry, uniform, fine sand were prepared. Figure 6 shows Model T3, which was investigated by Lanazo. The linear variable differential transformers (LVDTs) were positioned at different points of the model to allow investigation of the changes in displacement.

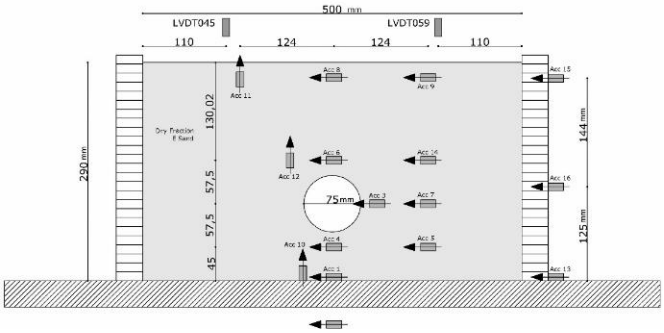

Figure 6 Physical model layout (Lanzano et al., 2012)

The model was 500 × 290 mm in size with a friction angle of 32° and aluminum alloy elastic modulus of 70 GPA. The physical model was simulated in a FE environment and was subjected to a dynamic load. The soil and seismic load characteristics were chosen according to the source research. The FE model of 500 mm in width and 300 m in height was constructed to simulate the exact dimensions of the physical test. Also, 15-node triangular elements and a Mohr-Coulomb soil model was used to simulate the soil behavior. Figures 7 and 8 show the time-history graphs of the dynamic load and the numerical model, respectively. The acceleration coefficient was 80g in accordance with the base research.

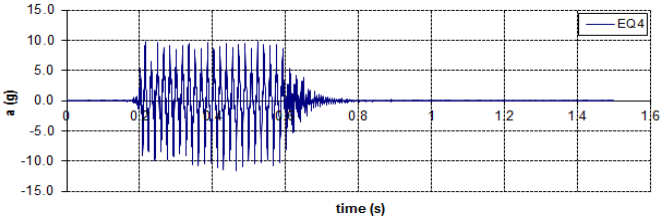

Figure 7 Time-history graph applied to centrifuge and FE model

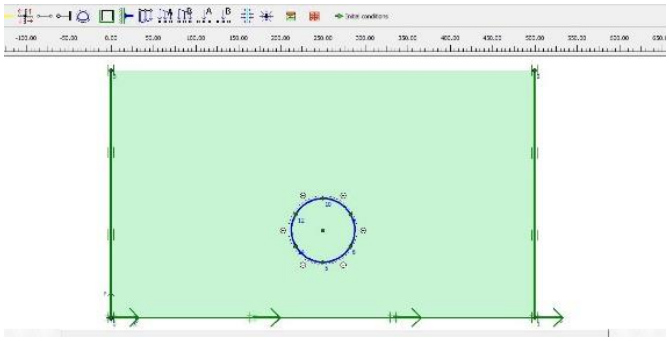

Figure 8 Simulation of physical model of centrifuge in FE environment

The total deformation changes at LVDT 045 (ground surface) were selected and the results were extracted in numerical analysis. To achieve the appropriate results, the shear modulus was selected as 27 MPa. The outputs of the numerical and the physical model are shown in Figures 9 and 10, respectively.

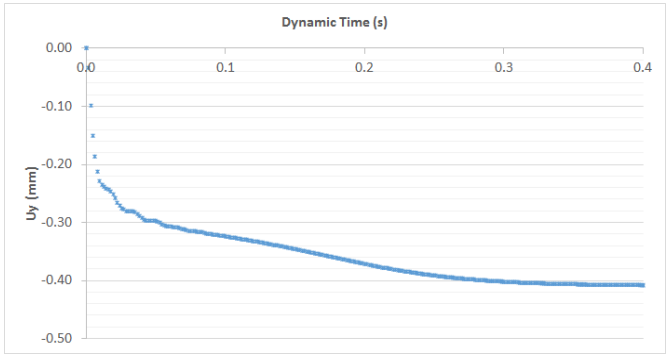

Figure 9 Total displacement at surface in FE analysis (LVDT 045)

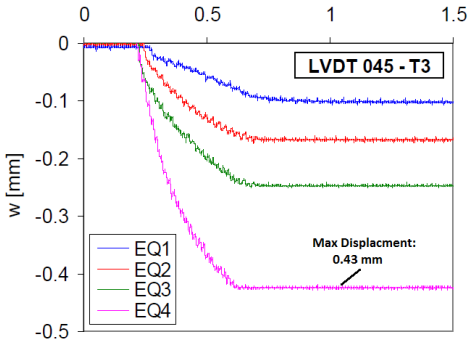

Figure 10 Total displacement at surface in physical model (LVDT 045)

The lining of the structure was modeled as a cluster in an elastic behavior model. Three structural ratios were analyzed at H/L values of 1, 1.5, and 2. It was not possible to investigate higher ratios due to static instability. The modeling was done using eight time-histories of shaking (four far-field and four near-field) for four friction angles (25°, 30°, 35°, 40°) and three dimension ratios (1, 1.5, 2), for a total of 96 simulations.

In the numerical model, the geometry of the model was divided into finite elements in order to perform FE calculations. Creating a mesh requires a general meshing parameter that shows the average element size (le). This parameter was defined in PLAXIS using the external geometric dimensions (Xmin, Xmax, Ymin, Ymax) and general coarse-grained settings as:

$$\text{average element size} < \frac{1}{8} \times \frac{V_{s,min}}{f_{max}}$$

$$l_e = \sqrt{\frac{(X_{max} - X_{min})(y_{max} - y_{\min})}{n_e}} \quad (1)$$

where ne is the number of elements in the model. In dynamic analysis, the following condition must be satisfied:

$$\text{average element size} < \frac{1}{8} \times \frac{V_{s,min}}{f_{max}} \quad (2)$$

where $V_{s,min}$ is the lowest shear wave velocity propagated in the layers and f_{max} is the maximum input wave frequency with a minimum value of en for mesh size. In order to investigate the stress changes, five points were selected on the structure and their shear stress data was extracted. The locations of these points are shown in Figure 11.

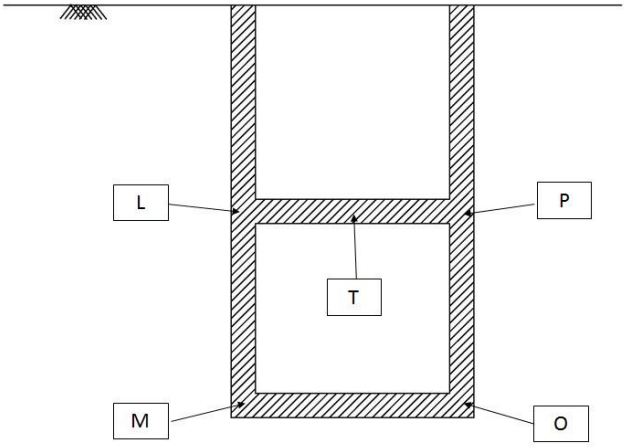

Figure 11 Location of selected points for investigating stress changes

2.4 Time History Analysis Parameters

In earthquake problems, dynamic loading is applied to the model bed as a function of time. The acceleration of gravity is considered to be 9.81 by default. In the dynamic analysis, the units are set in seconds. Absorbing boundaries are used in the dynamic analysis to prevent reflection of the earthquake waves. These boundaries are able to absorb the increasing stresses on the boundaries caused by the dynamic loads.

In dynamic analysis, the damping values must be specified as input to the software. The following parameters are required to determine the damping matrix:

- Newmark alpha and beta: These parameters for the manual settings in the iterative method determine the numerical time integral according to the implicit Newmark design. In order to obtain an unconditional constant answer, these parameters must satisfy the following relations:

$$025(.5 + \beta)^2 \leq \alpha \qquad 0.5 \leq \alpha$$
$$\alpha = 0.25 \qquad \beta = 0.5 \quad (3)$$

- C1 and C2 boundaries: C1 and C2 are relaxation coefficients to improve wave absorption on the absorbing boundaries. C1 corrects scattering in the direction perpendicular to the boundary and C2 corrects it in the tangent direction. If the boundaries are only perpendicular to the pressure waves, they do not have the required relaxation (C1 = C2 = 1). When the pressure wave is applied as an input to the model, the values

recommended by the software can be used (C2 = 0.25 and C1 = 1).

- Rayleigh alpha and beta: These parameters should be calculated and applied to the model separately for each earthquake and each soil type.

The hysteresis damping of the soil is independent of the frequency; however, there are drawbacks to its use in dynamic analysis. First, many simple hysteresis functions do not dampen all components equally when exposed to multiple waves. Second, the hysteresis functions are basically dependent on the stress path, which makes it difficult to interpret the results. Ideally, if a behavioral model can accurately represent the true hysteresis behavior of the soil, no additional damping will be required.

Often, the use of nonlinear behavioral models that can incorporate hysteresis damping into the model is problematic. In some cases, the model is unable to provide this type of damping and mechanical damping is used to investigate the dynamic behavior of the structure.

Rayleigh damping is the most common type of mechanical damping used in dynamic analysis. In time-domain applications, Rayleigh damping generally is used to provide damping which is almost independent of frequency. Although by definition, Rayleigh damping is dependent on frequency, its parameters can be used in a domain that minimizes the effects of frequency dependence as much as possible.

Rayleigh damping is generally used to dampen the natural oscillatory modes of the system in the analysis of structures and elastic continuous mediums. The equations are expressed in matrix form as follows:

$$C = \alpha_R M + \alpha\beta_R K \tag{4}$$

$$\alpha = 2\omega_a\omega_b\xi\frac{\omega_b - \omega_a}{(\omega_b^2 - \omega_a^2)} \tag{5}$$

$$\beta = 2\xi\frac{\omega_b - \omega_a}{(\omega_b^2 - \omega_a^2)} \tag{6}$$

$$\omega_a = \frac{\pi V_S}{2H} \tag{7}$$

$$f = \frac{1}{T}\ ,\omega_b = 2\pi f \tag{8}$$

$$f = \frac{V_S}{4H} \tag{9}$$

In which α and β are the Rayleigh damping coefficients where α is a mass-dependent damping coefficient and β is the hardness that is the dependent damping coefficient. Numerous studies have been done to select this frequency. Hudson (1994) suggested calculating the primary frequency as:

$$\omega_i = \frac{\pi V_s}{2H} \tag{10}$$

where ωi and ωj or ωa and ωb are the fundamental rotational speeds of the medium in the corresponding vibrations. The secondary rotational speed of ωj is estimated as nωi, where n is the first odd number greater than the ratio of the fundamental stimulus frequency and the natural frequency of the medium.

The minimum damping coefficient (ξmin) occurs at the minimum natural frequency point. In this case, the contributions of mass-dependent and hardness-dependent damping are the same. As the inherent damping is independent of frequency, the amplitude of the presented frequencies can be defined such that damping is practically constant. To do this, the low range of the Rayleigh damping curve can be used, where the damping value is relatively constant.

3. NUMERICAL MODELING RESULTS

After applying the time-history of each earthquake to the different geometries of the model, the stress value was read at the five specified points. Shear stress can be a suitable criterion for identifying conditions and how the structural mass fails. Figure 12 shows the maximum shear stress for the structure at φ = 25° and H/L = 1 for far-field earthquakes.

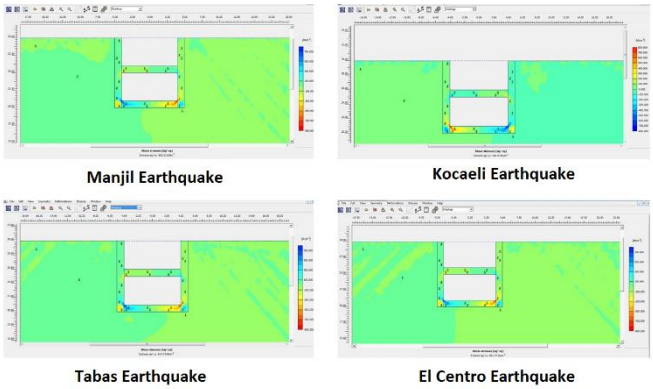

Figure 12 Maximum shear stress in time-history analysis at φ = 25°

The maximum shear stress for the different ratios of the structure and geotechnical conditions are presented in Tables 2 and 3. As the internal friction angle increased, the soil stiffness climbed and the stress created in the concrete structure decreased.

Table 2 Maximum shear stress in far-field earthquakes (kPa)

Earthquakes	Friction angle	H to L Ratio		
		H/L = 1	*H/L* = 1.5	*H/L* = 2
Manjil PGA = 0.184g	φ = 25	851.61	1140	2230
	φ = 30	839.57	1100	1900
	φ = 35	816.42	958.15	1480
	φ = 40	807.87	944.04	1450
Kocaeli PGA = 0.132g	φ = 25	790.97	1110	2060
	φ = 30	752.45	1060	1780
	φ = 35	736.48	925.98	1520
	φ = 40	712.96	929.04	1500
Kobe PGA = 0.15g	φ = 25	947.42	1160	2460
	φ = 30	924.86	1110	2180
	φ = 35	896.36	978.5	1820
	φ = 40	835.53	976.22	1860
Chi Chi PGA = 0.094g	φ = 25	897.19	1070	2080
	φ = 30	860.21	1020	1950
	φ = 35	835.63	919.33	1640
	φ = 40	796.54	897.6	1580

Table 3 Maximum shear stress in near-field earthquakes (kPa)

Earthquakes	Friction angle	H to L Ratio		
		H/L = 1	*H/L* = 1.5	*H/L* = 2
Landers PGA = 0.164g	φ = 25	772.12	1140	2420
	φ = 30	745.04	1090	2100
	φ = 35	732.67	1010	1460
	φ = 40	713.66	1020	1440
Fruili PGA = 0.21g	φ = 25	741.94	980.67	1920
	φ = 30	728.85	948.46	1780
	φ = 35	721.72	885.87	1520
	φ = 40	719.82	892.77	1490
Tabas PGA = 0.324g	φ = 25	814.75	1070	2040
	φ = 30	801.33	1020	1900
	φ = 35	784.76	927.68	1630
	φ = 40	759.49	923.48	1640
El Centro PGA = 0.281g	φ = 25	821.73	1010	2160
	φ = 30	797.84	995.82	1890
	φ = 35	781.81	905.99	1610
	φ = 40	763.53	892.48	1500

The shear resistance of concrete can be calculated as:

$$Vc = 0.53 \times \sqrt{f'c}\, bw\, d\ (kg)$$
$$Vc = 0.53 \times \sqrt{300} = 9.18\ kg/cm^2 = 900\ kPa \quad (11)$$

where fc is the uniaxial of concrete strength and bw and d are the width and depth of the concrete element, respectively. In almost all cases, when H/L increased above 1.5, the shear stress exceeded the shear resistance of the concrete, which indicates the failure of the structure.

The maximum shear stress also affected the stability of the structure. The results of the analysis were extracted and investigated at the specified points. Figures 13 to 16 show that, as the internal friction angle increased at points L and P (in proximity to the middle wall), the normal stress increased as well. This trend continued for all far-field earthquakes up to an internal friction angle of 35° and then decreased. Somewhat different changes can also be observed for near-field earthquakes.

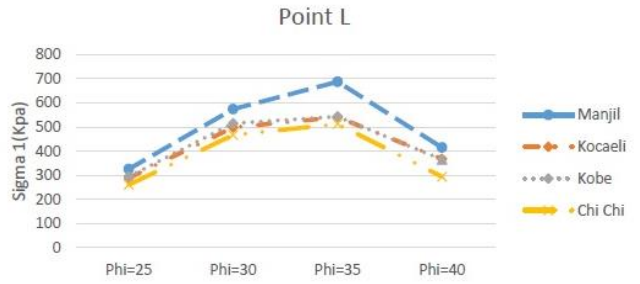

Figure 13 Normal stress changes in time-history analysis for far-field earthquake at H/L = 1

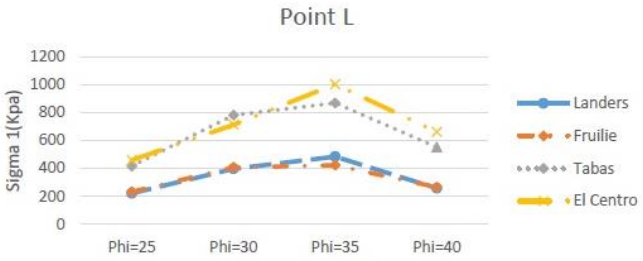

Figure 14 Normal stress changes in time-history analysis for near-field earthquake at H/L = 1

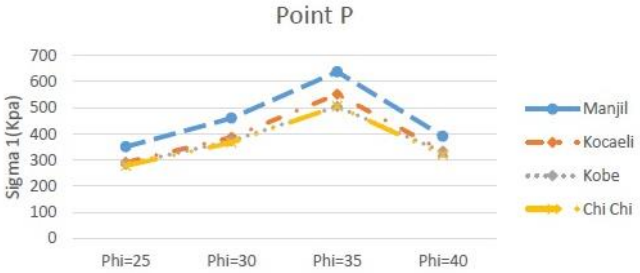

Figure 15 Normal stress changes in time-history analysis for far-field earthquake at H/L = 1

At a friction angle of φ = 25°, as structural ratio H/L changed from 1 to 1.5, the shear stress grow up at least 20%. As H/L increased from 1.5 to 2, the minimum rise in stress was 85%. At higher internal friction angles, the trend of change in the stress at the endpoints of the wall was low and almost independent of the friction angle. The conditions at the heel points of the structure at φ > 25° decreased significantly. Figures 19 and 20 show that the trend was almost the same for both the far- and near-field earthquakes. Most of the variation in shear stress occurred with a change in the internal friction angle at the midpoint of the wall and at mid-beam. No significant change was observed in the rest of the structures. Figures 21 to 24 show the variation in shear stress at points P and T as representative of the midpoints of the wall and beam.

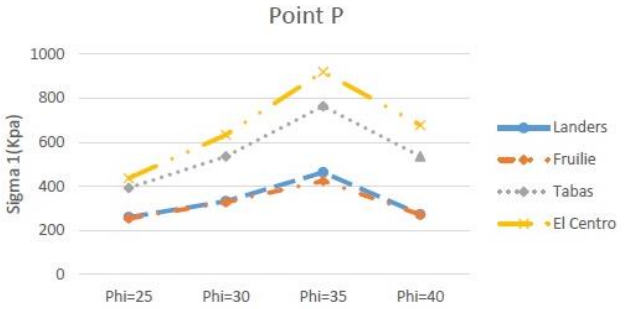

Figure 16 Normal stress changes in time-history analysis for near-field earthquake at H/L = 1

The drop in stress beyond φ = 35 could be due to the increase in the shear resistance of the soil mass and decrease in the relative stiffness between the structure and soil. At the intersection points of the wall and floor of the structure (M, O), the stress changes at values higher than φ = 30 stopped and the diagram flattened (Figures 17 to 20).

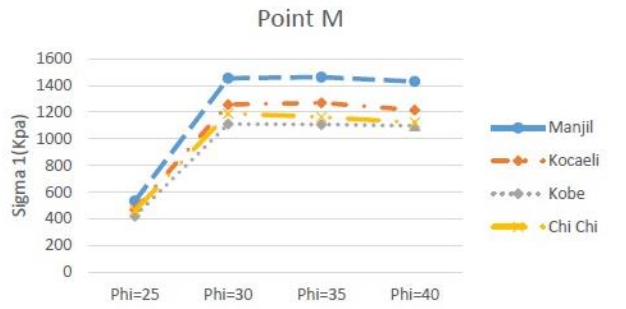

Figure 17 Normal stress changes in time-history analysis for far-field earthquake at H/L = 1

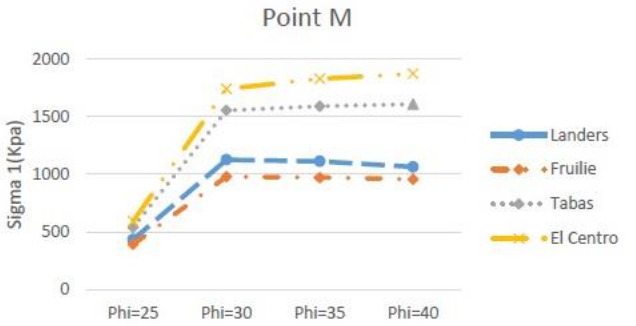

Figure 18 Normal stress changes in time-history analysis for near-field earthquake at H/L = 1

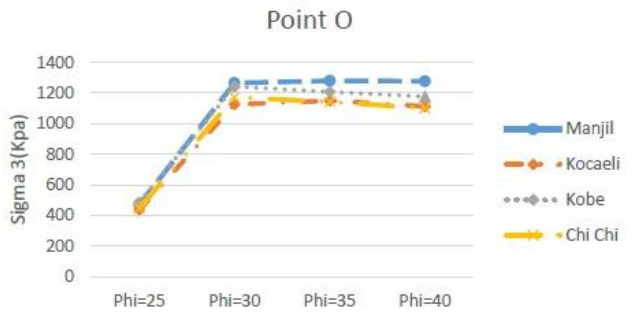

Figure 19 Normal stress changes in time-history analysis for far-field earthquake at H/L = 1

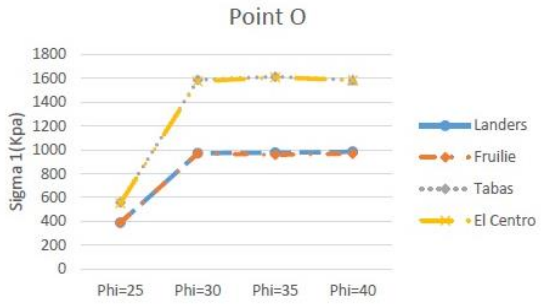

Figure 20 Normal stress changes in time-history analysis for near-field earthquake at H/L = 1

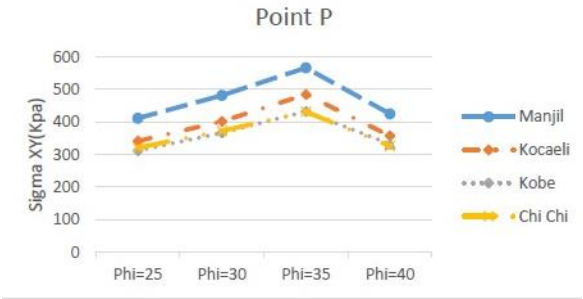

Figure 21 Shear stress changes in time-history analysis for far-field earthquake at midpoint of wall and H/L = 1

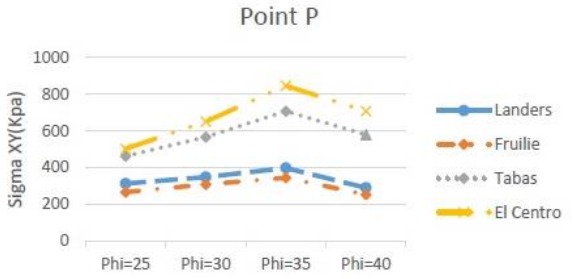

Figure 22 Shear stress changes in time-history analysis for near-field earthquake at midpoint of wall and H/L = 1

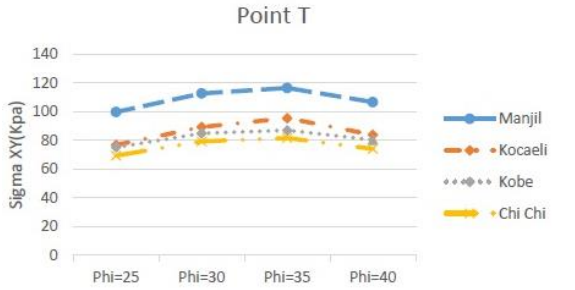

Figure 23 Shear stress changes in time-history analysis for far-field earthquake at midpoint of wall and H/L = 1

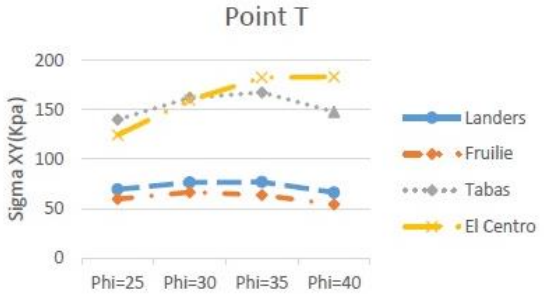

Figure 24 Shear stress changes in time-history analysis for near-field earthquake at midpoint of wall and H/L = 1

As can be seen, changes in shear stress under the influence of near-field earthquakes were much less than for far-field earthquakes. The absolute stress for the near-field earthquakes at maximum acceleration were greater than for the far-field earthquakes (such as Kobe and El Centro). This could be because of the higher PGA in near-field earthquakes.

As the H/L ratio of the structure increased, the values and trend of stress variation changed drastically. At point L, the lowest stress and changes were at H/L = 1 and, as H/L increased, the shear stress and intensity of change also climbed up. The 3D diagrams in Figures 25 and 26 show the shear stress changes caused by the changes in the dimensions of the structure from time-history analysis for far-field and near-field earthquakes.

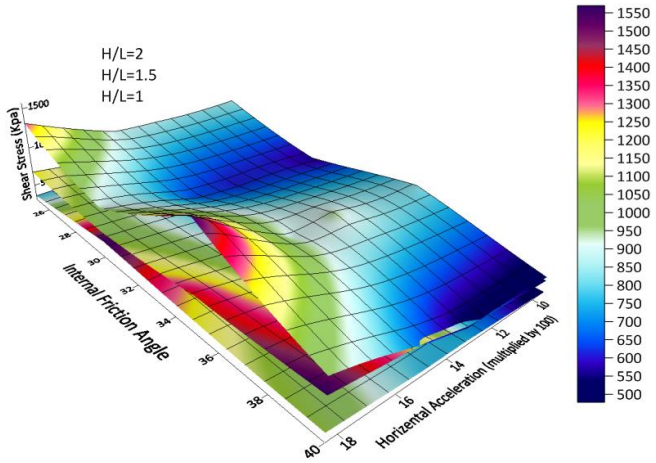

Figure 25 Shear stress changes in time-history analysis for far-field earthquake for geometry change in model, point L

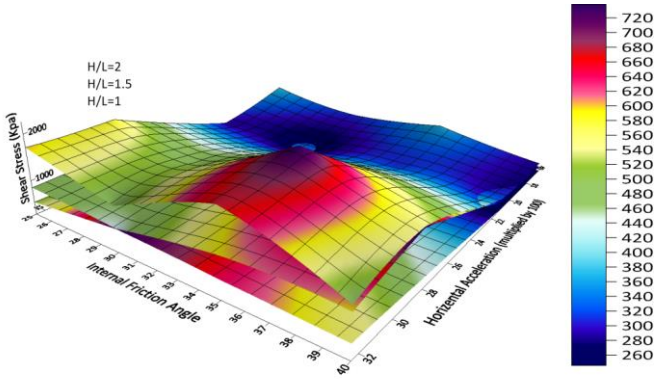

Figure 26 Shear stress changes in time history analysis of near-field earthquake for geometry change in model, point L

The intensity of shear stress changes at H/L = 1.5 and 1 were different from each other. At H/L = 1.5 beyond an internal friction angle of 35°, the stress rise significantly. In far-field earthquakes, as the horizontal acceleration coefficient growth, the amount of stress increased and reached a maximum at φ = 35°. For near-field earthquakes, the maximum stress occurred at a = 0.28g (H/L = 2), which could have been related to the frequency content. As a constant dimension ratio, the mode of stress changed. At H/L = 1, the maximum stress occurred at maximum horizontal acceleration and φ = 30° (Figure 27).

As shown in Figures 17 to 20, at the intersection of the wall with the floor of the structure (point M), the normal stress changes were greater than the shear stress changes as the dimensions of the structure increased. The trend of change in shear stress were very similar and almost independent of the internal friction angle. Sigma 1 changed as the friction angle changed. In Figure 28 shows the shear stress versus the model geometry. At a constant dimension ratio (H/L = 1) under the influence of a far-field earthquake, the mode of stress changed at

point M to become nearly the same as at Point L and maximum stress occurred at the maximum horizontal acceleration. In the case of near-field earthquakes, extreme stress occurred at a = 0.28g and increased as the internal friction improved (Figure 29).

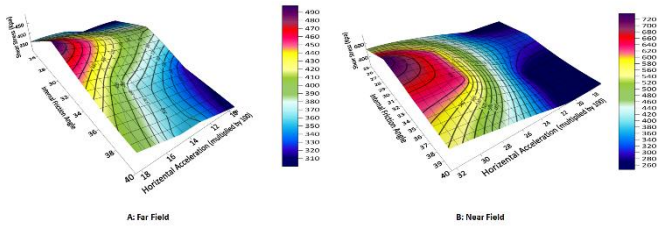

Figure 27 Shear stress changes in time-history analysis for constant geometry at H/L = 1, point L

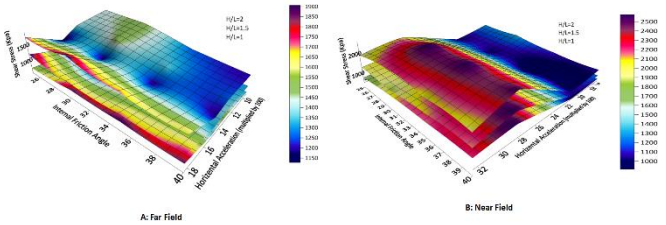

Figure 28 Shear stress changes in time-history analysis for geometry change in model, point M

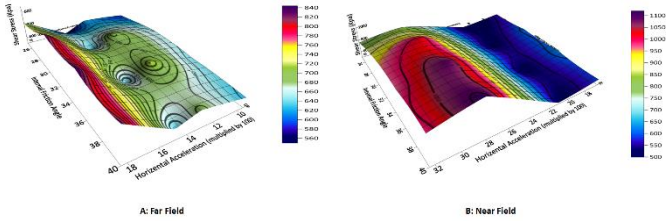

Figure 29 Shear stress changes in time-history analysis for constant geometry at H/L = 1, point M

In far-field earthquakes, the maximum shear stress was for the Manjil earthquake, which had the strongest horizontal acceleration. However, for near-field earthquakes, the maximum amounts were for the El Centro earthquake, which could relate to the frequency content of the earthquake (Figure 30).

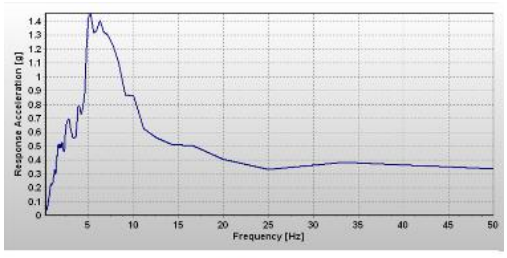

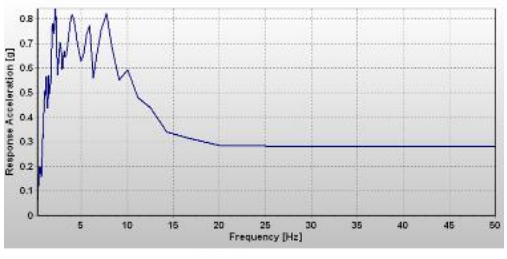

Figure 30 Content frequency of near -field earthquakes

At mid-beam, as shown in Figures 31 and 32, the shear stress under all geometrical conditions increased independently from the internal friction angle in far-field earthquakes. In other hand, in near-field earthquakes rising the internal friction angle has caused higher value of stress concentration.

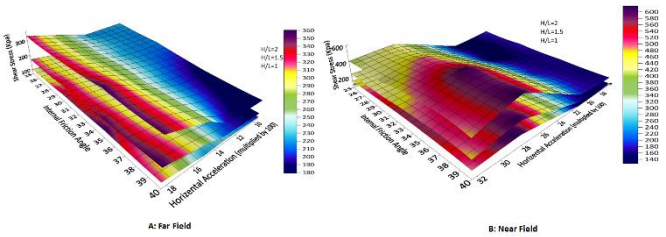

Figure 31 Shear stress changes in time history analysis for geometry change in model, point T

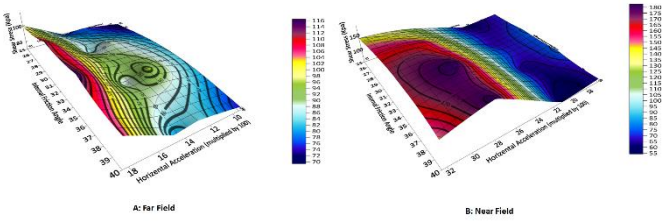

Figure 32 Shear stress changes in time history analysis for constant geometry H/L = 1, point T

At a dimension ratio of H/L = 1 for far-field earthquakes, the increase in shear stress depended directly on the horizontal acceleration and remain unchanged against changes in the internal friction angle. For near-field earthquakes, the shear stress was a function of the horizontal acceleration. At a PGA > 0.22g, the stress rise as the internal friction angle increased.

4. CONCLUSIONS

The present study investigated the dynamic behavior of H-shaped combined underground surface and complex underground structures as influenced by far-field and near-field earthquakes. Three geometries with H/L ratios of 1, 1.5, 2 were selected as the target structures. The analyses were conducted for granular soil with internal friction angles of 25° to 40° (in 5° increments). Five points on the structure were selected as history points and the shear stress values were extracted.

A decrease in shear stress was observed at all structural ratios with an increase in the internal friction angle. In almost all earthquakes, beyond an internal friction angle of 25°, the shear stress caused by the dynamic load exceeded the shear resistance of the concrete wall (about 900 kN), which indicates structural failure. For internal friction angles of 35° to 40°, the decrease in shear stress was very low and, in some cases, was unchanged. This was due to the improvement on soil hardness and the resulting increase in soil shear resistance. Moreover, in the near-field earthquakes, the maximum amounts were for the El Centro earthquake, which is a result of the frequency content of the earthquakes.

At constant friction angle ($\varphi = 25°$), as the structural ratio vary from 1 to 1.5, the shear stress increase by rising H/L to 2, the stress added 85%, which indicates the strong effect of the dimensions on the induction stress. At higher internal friction angles, the rate of change in stress decreased as the structural ratio increased. The trend of shear stress changed at the endpoints of the wall was almost independent from the internal friction angle. However, the conditions at the heel points of the structure at $\varphi > 25°$ declined significantly.

At the heel of the structures (point M) and the midpoint of the beam (point T), at a constant dimension ratio, in the higher acceleration ratio, the amount of shear stress increased. In far-field earthquakes, the change in shear stress was a function of growth in horizontal acceleration and was almost independent from internal

friction angle. For near-field earthquakes, the shear stress was a function of the horizontal acceleration as well as the internal friction angle. In all cases, an increase in the geometric dimension ratio of the structure caused a higher values in the stress.

It was found that the effect of change in the H/L ratio of the structure was more effective than the internal friction angle on the change in stress. Generally, in far-field earthquakes, the shear stress was only a function of the horizontal acceleration and H/L ratio. In near-field earthquakes, it was a function of the frequency content and the internal friction angle. It is suggested to investigate the validity and proficiency of quasi-static methods, such as Hashash and Mono nobe okabe, in future research.

5. REFERENCES

ASCE (1974) “Earthquake damage evaluation and design considerations for underground structures”, American Society of Civil Engineers, Los Angeles Section.

Brinkgreve, R.B.J., Engin, E. and Swolfs, W.M. (2015) Manual Plaxis 2D / 3D. Plaxis BV, Delft.

Cakir, T. and Livaoglu, R. (2012) “Fast practical analytical model for analysis of backfill rectangular tank fluid interaction systems", Soil Dynamics and Earthquake Engineering, vol.37, pp24-37.

Dobashi, H., Hatsuku, T., Ichimura, T., Hori, M., Yamada, T., Ohbo, N., Moriguchi, M., and Itami, H. (2008) “Full 3d seismic response analysis of underground ramp tunnel structure using large-scale numerical computation”, the 14th world conference on earthquake engineering, Beijing, China.

Duncan, J. M., and Chang, C. Y. (1970) "Nonlinear analysis of stress and strain in soils", Journal of the Soil Mechanics and Foundations Division, ASCE, Vol. 96, pp1629-1653.

Hashash, Y.M.A., and Hook, J.J., Schmidt, B., and Yao, J.I-C. (2001) “Seismic design and analysis of underground structure”, Tunnelling and Underground space Technology 16, pp247-293.

Lanzano, G. (2012) “Physical and analytical modelling tunnels under dynamic loadings”, PhD Thesis, University of Napoli.

Mononobe, N. (1929) “On determination of earth pressure during earthquake”, InProc. World Engineering Congress Vol. 9, pp177-185.

Nadim, F. (1982) “A numerical model for evaluation of seismic behavior of gravity retaining walls”, Massachusetts Institute of technology.

Nordal, S. (2016) “Geotechnical engineering advanced course: Lecture notes and background material”, NTNU, Geotechnical Division, Trondheim

Okabe, S. (1926) “General theory of earth pressure”, J. of the Japanese Society of Civil Engineers, Tokyo, Japan.12(1).

Okamoto. (1984) “Introduction to earthquake engineering”, University of Tokyo press.

Owen, G.N., and Scholl, R.E. (1981) “Earthquake engineering of large underground structures”, Report no. FHWA_RD-80_195. Federal Highway Administration and National Science Foundation.

Penzien, J. (2000) “Seismically induced racking of tunnel linings”, Int. J. Earthquake Eng. Struct. Dyn. 29, pp683-691

Schanz, T., Vermeer, P. A., and Bonnier, P. G. (1999) "The hardening soil model: formulation and verification", Beyond 2000 in Computational Geotechnics, Balkema, Rotterdam.

Seed, H.B., Wong, R.T., Idriss, I.M., Tokimatsu, K., and Moduli. (1992) “Damping factors for dynamic analyses of cohesionless soils”, Journal of geotechnical engineering.112(11): pp1016-32

Sharma, S., and Judd, W.R. (1991) “Underground opening damage from earthquakes”, Eng. Geol. 30, pp263-276.

Sherif, M.A., Fang, Y.S., Sherif, R.I., KA and Ko. (1984) “Behind rotating and non-yielding walls”, Journal of Geotechnical Engineering. 110(1), pp41-56.

Wang, J. N. (1993) “Seismic Design of Tunnels: A state-of-the-art Approach”, Parsons Brinckerhoff Quade and Douglas, Inc